Available online at www.sciencedirect.com
SCIENCE DIRECT®
Catalysis Today 96 (2004) 61–70
CATALYSIS TODAY
www.elsevier.com/locate/cattod

Coated bifunctional catalysts for NO_x SCR with C_3H_6 Part II. In situ spectroscopic characterization

Mario J. Castagnola, Michael K. Neylon[1], Christopher L. Marshall*

Chemical Engineering Division, Argonne National Laboratory, Argonne, IL 60439, USA

Available online 25 June 2004

Abstract

The effect of finely coating Cu-ZSM-5 with nanoparticles of ceria has been studied in situ by XANES, DRIFTS and TPR. The combination of these techniques reveals a lower temperature of reduction for both metals (Cu and Ce) in the bifunctional catalyst. Copper interacts with ceria nanocrystals at the oxide–zeolite interface and forms a localized phase comparable to doped ceria solid solutions commonly used as oxidation catalysts. As a result the catalyst is able to activate C_3H_6 and form NO_2 at low temperatures. Analysis of the stability of adsorbed CO by DRIFTS suggests that the addition of water promotes the oxidation of Cu^{1+} on the coated catalyst. In addition, TPD and TGA results, in combination with supplementary DRIFTS experiments, indicate that the ceria coating retains water at the interface during reaction conditions. The combination of these events yields relatively high C_3H_6-SCR activity at temperatures as low as 250 °C. It is believed that the affinity towards water and extended coverage of the coating also protects the zeolite against degradation by restricting the diffusion of water molecules into the zeolite pores.

Keywords: Cu-ZSM-5; CeO_2; Lean burn; deNOx; Low temperature; Propylene; TPR; Infrared; X-ray absorption; Water effect

1. Introduction

The reduction of nitric oxide to dinitrogen typically involves two main steps: the oxidation of NO to NO_2 and the reduction of NO_2 to N_2. Single catalysts, such as Cu-ZSM-5 or Pt/Al_2O_3, have the ability to perform these two tasks sequentially [1,2]. Researchers have also approached this set of reactions with bifunctional catalysts. In this type of materials an active component is optimized for the oxidation of NO while a second component is reserved for the final reduction of NO_2. That is the case for two metals co-impregnated on a support, zeolites co-exchanged with two metals, or even, physical mixtures of catalysts. When the two reactions are suitably overlapped, an enhancement in activity not observed in the individual components can be produced.

Cerium oxide is known to promote oxidation reactions, including the oxidation of NO to NO_2. Bifunctional catalysts have been produced by adding cerium to zeolites known to catalyze NO_x reduction. Different approaches have been used to accomplish this bifunctionality. Some include cerium ions co-exchanged in Cu-ZSM-5 for NO decomposition and in Ag-ZSM-5 for CH_4-SCR [3,4]. In other cases, composites of ceria and In-ZSM-5 have been prepared via physical mixtures or precipitation of cerium hydroxide onto the surface of the zeolite for CH_4 and C_3H_8-SCR [5]. The results vary with the type of reaction. In some cases the temperature of maximum activity is lowered by about 50 °C relative to the unmodified catalyst, while in others the activity at high temperature is enhanced. Longer stability towards hydrothermal zeolite degradation has also been reported.

Our group has recently reported a novel approach for the preparation of this type of bifunctional catalysts [6]. By impregnating a metal-exchanged zeolite with a metal oxide colloidal sol, a fine coating of oxide is produced on the zeolite surface. The method produces not only a unique topology and physical structure of the catalyst at the submicron level but also maximizes the benefits already observed in other materials with similar active component combinations. In particular, CeO_2/Cu-ZSM-5 prepared this way shows a temperature drop for its activity maximum of 150 °C under wet C_3H_6-SCR conditions relative to the

* Corresponding author.
E-mail address: clmarshall@anl.gov (C.L. Marshall).
[1] Present address: Nu Element, Inc., 2323 N. 30th Street, Suite 100, Tacoma, WA 98403, USA.

0920-5861/$ – see front matter © 2004 Elsevier B.V. All rights reserved.
doi:10.1016/j.cattod.2004.05.001

native Cu-exchanged zeolite. As in other combinations of Cu-ZSM-5 and cerium, the coated catalyst also shows better stability than Cu-ZSM-5 towards hydrothermal zeolite degradation. In addition, the deNO_x activity displayed by the coated catalyst is enhanced in the presence of water, which is a unique property among modified Cu-ZSM-5 catalysts.

In this work the interaction of the active components in the coated system is studied by different in situ spectroscopic techniques, including X-ray absorption near edge spectroscopy (XANES) and diffuse reflectance infrared Fourier transform spectroscopy (DRIFTS). Coupled to other standard analytical techniques such as temperature programmed reactions (TPR) and thermogravimetric analysis (TGA), the means by which this catalytic system displays the observed benefits are established.

2. Experimental

2.1. Materials

NH_4-ZSM-5 with a Si/Al ratio of 25 was provided by Zeolyst International. To obtain the H-forms, the zeolite was calcined at 550 °C for 4 h in a static furnace. Cu-ZSM-5 was prepared by ion-exchanging H-ZSM-5 according to commonly used literature procedures. A 100 mL solution of 0.01 M $Cu(NO_3)_2{\cdot}2.5H_2O$ (99.99%, Aldrich) was stirred vigorously with 10 g of H-ZSM-5 for 2 h before adjusting the pH dropwise to 8 using a 0.8 M NH_4OH (30%, AR, Mallinkrodt) solution while stirring. The slurry was stirred for an additional 24 h. Then the solid was filtered, rinsed with water and dried at 100 °C. Samples were calcined for 4 h at 450–500 °C. The exchange step was performed two more times until about 120–130% exchanged Cu-ZSM-5 was obtained (following the commonly used nomenclature where 100% exchanged stands for one Cu ion per every two Al sites).

Ceria was added to the zeolite by incipient wetness impregnation of a colloidal sol. In this work, ceria typically accounted in all samples of CeO_2/Cu-ZSM-5 for an additional 24 wt.%, except when noted. To prepare a 24% CeO_2/Cu-ZSM-5 catalyst, 1.1 mL of CeO_2 sol (20%, Nyacol, acetate stabilized) used to impregnate 1 g of Cu-ZSM-5 under constant mechanical mixing. After drying at 100 °C, the solid sample was calcined at 500 °C for 4 h. A similar procedure was followed to prepare CeO_2/H-ZSM-5 out of H-ZSM-5.

Preparation of a sol of CeO_2 doped with Sm or Zr was achieved by combining 0.08 M solutions of $Ce(NO_3)_3$ and $Sm(NO_3)_3$ or $ZrONO_3$ (Aldrich), in the desired ratio, followed by precipitation of the hydroxide with concentrated NH_3 (30%, AR, Mallinkrodt). The solid was filtered, washed two times with nanopure water and one time with ethanol, air-dried and dried in a vacuum oven overnight at 110 °C. The samarium-doped ceria was peptized with 0.6 M acetic acid at room temperature. The zirconia doped material was peptized with an equimolar mixture of diluted nitric acid in a Parr bomb at 135 °C. The colloidal mixtures were diluted in water to the desired concentration, ultracentrifuged and filtered through a 0.2 μm membrane. Impregnation of Cu-ZSM-5 with these colloidal dispersions yielded 15% $Ce_{0.8}Zr_{0.2}O_2$/Cu-ZSM-5 and 10% $Ce_{0.8}Sm_{0.2}O_{1.9}$/Cu-ZSM-5.

2.2. Characterization

All gases used in the different characterization procedures were supplied by AGA. Temperature programmed reduction (TPR) was performed on an Altamira AM-1 unit equipped with a thermal conductivity detector (TCD). The outlet gases were also analyzed by a Stanford Research Residual Gas Analyzer (RGA, mass spectrometer). Approximately, 150 mg of sample were loaded into a 1/8-in. quartz U-tube and installed on the unit. Prior to the TPR runs, samples were pretreated in 30 sccm O_2/He (5%) at 500 °C for 30 min, and then cooled to room temperature. Samples were heated to 800 °C under a flow of 30 sccm of H_2(4%)/Ar (He for TPD). A temperature ramp of 5 °C/min was used.

In situ X-ray absorption spectroscopy (XAS) studies were performed at the Materials Research Collaborative Access Team (MR-CAT) beamline (10-ID) at the Advanced Photon Source (APS), Argonne National Laboratory. Cu-K and Ce-L_3 edge XAS spectra were collected in transmission mode, with the X-ray beam passing through ionization chambers filled with N_2 before and after the sample cell. The energy was selected with a cryogenic double-crystal Si (1 1 1) monochromator; an uncoated glass mirror reduced higher order harmonics. Approximately, 20 mg of up to four samples were loaded as self-supporting wafers into a 0.50 in. multi-sample metal holder with four individual 0.16 in. diameter holes. The holder was placed into a quartz sample tube (3/4 in. o.d.), centered in a clam shell furnace, described by Neylon et al. [7]. The sample temperature was measured by a thermocouple positioned near the sample holder inside the quartz tube. Before moving the sample cell onto the beamline, the samples were treated off-line in air (TPR) or H_2 (4%) in He (TPO) up to 500 °C for at least an hour. Once on-line, the four samples were scanned sequentially using a precision motion stage. The samples in the cell were heated up to 600 °C with a temperature ramp of 2 °C/min under a 30 sccm flow of H_2 (4%) in He (TPR) or dry air (TPO). Scans of all samples were recorded every 2–3 min during the reaction with 40–60 spectra per sample collected during each run. In addition, a Cu foil reference spectrum was collected for energy calibration using a third ionization chamber.

Factor analysis was used to analyze the data from the TPR and TPO runs in the XANES region of the Cu and Ce edges [7]. The energy of the Cu-edge spectra was calibrated using the reference Cu foil transmission spectrum to better than ±0.05 eV relative offset. The spectra were normalized and cubic splines were used to convert each spectrum to a

constant energy grid at 0.5 eV increments. The normalized discrete data was collected in a matrix, and singular value decomposition was used to find the associated eigenvalues and eigenvectors. Iterative key set factor analysis (IKSFA) [8] was used to determine which of the initial XANES data sets were most fundamental, and the other data in the set were fitted using a least squares analysis on a linear sum of these fundamental vectors.

Diffuse Reflectance Infrared Spectroscopy was performed on a Bomem DA3 spectrometer equipped with a Harrick Scientific HVC-DRP low pressure, high temperature diffuse reflectance cell. BaF_2 windows (Harrick) were used when water was incorporated in the feed. Infrared radiation was produced by a Globar source. The reflected radiation was collected by a praying mantis optical attachment (Harrick DRA-2CE) and re-directed to a Mercury-Cadmium-Telluride detector (Bomem). The gas mixture of interest was blended on a manifold system upstream of the cell. Water was injected and vaporized directly into the chamber of the cell. For the experiments involving CO absorption, 1000 ppm of CO in nitrogen were used. When required, 8% O_2 and 6–10% H_2O were introduced. For experiments simulating C_3H_6-SCR conditions, 1000 ppm NO, 1000 ppm C_3H_6 and 8% O_2 in nitrogen were used. The feed (100 sccm) was forced to diffuse downflow through about 100 mg of sample loaded on a cup sitting on top of the heating cartridge of the cell. Neat samples were used to maximize the signal of the adsorbates. Samples were heated up to 400 °C. The walls and windows of the cell were protected from the heat by water jackets. A thermocouple was positioned in contact with the top surface of the catalyst. The dome of the cell maintained a controlled environment around the sample during the experiment. Spectra were collected with a resolution of 2.0 cm^{-1}. Quantitative analysis was performed on Kubelka–Munk traces after equilibrium had been reached. Reference files were collected of each catalyst before adsorption at each temperature of data collection.

Thermogravimetric analysis of samples was performed on a HAAKE EXSTAR 6000 TG/DTA instrument against an alumina standard between 20 and 600 °C. A flow of 100 sccm of nitrogen gas and a temperature ramp of 5 °C/min were used. Samples were placed overnight in a controlled environment under a water vapor saturated atmosphere.

2.3. Catalytic tests

Catalytic activity tests were performed in identical manner as previously described [6]. A microscale plug flow reactor was used to test the catalyst activity. Pure He (99.995%) and the gas mixtures 5% O_2 in He, 5% NO in He, and 3% C_3H_6 in He were obtained from AGA in Certified Grade. Gas flow rates were controlled using Brooks 5860E mass flow controllers to achieve a nominal gas concentration of 2% O_2, 1000 ppm NO and 1000 ppm C_3H_6, balance He at 100 sccm. Water was introduced, when used, through a syringe pump to achieve 10% by volume in the reactant feed; all lines after water introduction were heat traced until vented to prevent condensation. The sample mass was typically 150 mg, diluted up to 2 g using SiC (Electro Abrasive, 40 mesh, about 350 μm particle size) in order to increase the size of the bed and avoid heat transfer effects. The temperature of the catalyst was monitored by a thermocouple inserted in the catalyst bed and controlled using an Omega CN9000 temperature controller. A clam-shell furnace was used to maintain reaction temperatures between 150 and 600 °C.

The use of two analytical instruments allowed the monitoring of all common products of HC-SCR reactions. The NO and NO_2 concentrations were monitored on-line with a California Analytical Instruments Model 400-HCLD Chemiluminescence NO/NO_x analyzer. An internal heated pump prevented water condensation inside the instrument. An on-line MTI MicroGC 200, equipped with a thermal conductivity detector and two chromatographic columns, was used to analyze the other components of the effluent gas stream. N_2, O_2 and CO were separated on a Molecular Sieve 5A column (10 m) while a PoraPLOT U column (4 m) was used for CO_2, N_2O, hydrocarbons and water.

Pretreatment of the catalysts included heating the samples in situ at 500 °C under pure He for 1 h followed by 2 h at 250 °C under the reaction feed in order to approach pseudo-steady-state conditions. Measurements were taken after 15 min of stabilization and at least three points were taken at each temperature at 15 min intervals.

Thermodynamic calculations were performed with HSC Chemistry 5.11 software from Outokumpu Research Oy. For the O_2+NO to NO_2 reaction, values of 2% O_2 and 1000 ppm NO in He in the 25–1000 °C range at 25 °C intervals were used.

3. Results

3.1. SCR activity

The catalytic activity of Cu-ZSM-5 under wet C_3H_6-SCR conditions is shown in Fig. 1a. The maximum NO conversion is about 55–60% and the propylene conversion is about 100% at 400 °C under wet conditions. Considerable amounts of CO (22%) and N_2O (4%) are produced at temperatures lower than 400 °C and NO_2 (6%) above 350 °C.

Under the same conditions, the bifunctional CeO_2/Cu-ZSM-5 catalyst in Fig. 1b converts a maximum of about of 40–45% NO at 250 °C. Propylene conversion reaches 100% around this temperature as well. No significant amount of CO or N_2O is observed in the 150–550 °C range. At the high temperature range a large amount of NO_2 (18% at 400 °C) is formed.

3.2. TPR

Fig. 2 compares the results of the temperature programmed reduction of Cu-ZSM-5, CeO_2/H-ZSM-5 and

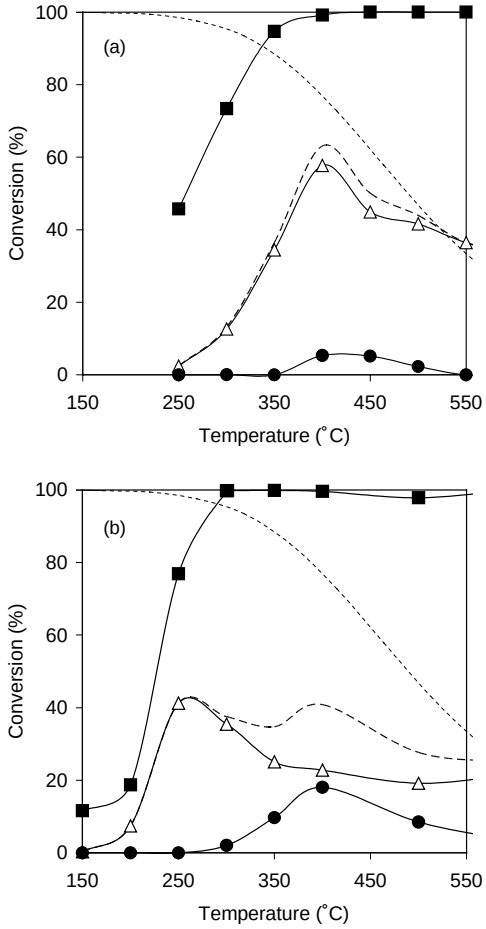

Fig. 1. Activity profile of (a) Cu-ZSM-5 and (b) CeO_2/Cu-ZSM-5. (■) Conversion of C_3H_6; (△) conversion of NO to N_2; (●) conversion of NO to NO_2. Conditions: 1000 ppm NO, 1000 ppm C_3H_6, 2% O_2, 10% H_2O, balance He. GHSV = 40,000 h^{-1} (based on mass of catalyst). Dashed line: total NO conversion ($N_2 + NO_2 + N_2O$). Dotted line: calculated NO_2 thermodynamic disappearance.

CeO_2/Cu-ZSM-5 under H_2 up to 750 °C. Cu-ZSM-5 shows two reduction events. The first occurs around 220 °C, corresponding to the reduction of Cu^{2+} to Cu^{1+}. The second event near 350–400 °C corresponds to the Cu^0 formation. Particles of CuO that may have formed due to excessive exchange reduce directly to Cu^0 near 210 °C.

Bulk CeO_2 typically shows two reduction peaks; one near 400 °C corresponding to the reaction of hydrogen with surface ceria oxygen. Bulk ceria oxygen reacts above 600 °C. These reduction events are observed in the case of CeO_2/H-ZSM-5, suggesting that there are significant quantities of a bulk-like CeO_2 phase on the sample.

In the case of CeO_2/Cu-ZSM-5 a reduction event occurs as low at 150 °C with a shoulder around 125 °C. However, no generation of water, based on the RGA results, is observed until past 160 °C. Peaks at 250 and 350–400 °C also are observed but in considerable lower magnitude compared to the parent Cu-ZSM-5. The sample also shows a small signal at 600 °C, probably corresponding to bulk CeO_2 reduction.

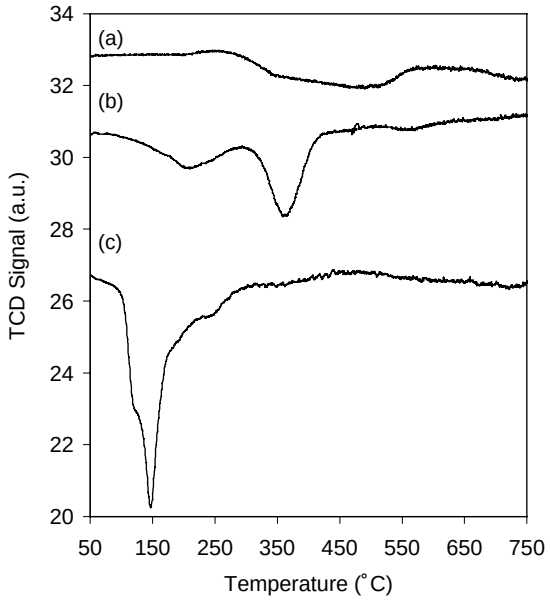

Fig. 2. TPR profile of (a) CeO_2/H-ZSM-5, (b) Cu-ZSM-5 and (c) CeO_2/Cu-ZSM-5. Conditions: 4% H_2 in Ar, flow = 30 sccm, temperature ramp = 5 °C/min.

Fig. 3 shows the reduction profiles of $Ce_{0.8}Sm_{0.2}O_{1.9}$/Cu-ZSM-5 and $Ce_{0.8}Zr_{0.2}O_2$/Cu-ZSM-5. The first reduction events for the Zr-doped sample occur at less than 150 °C. However, in both cases water formation is also observed only above 160 °C.

3.3. In situ XAS

The variation of the Cu K edge of Cu-ZSM-5 and the CeO_2/Cu-ZSM-5 as a function of temperature during

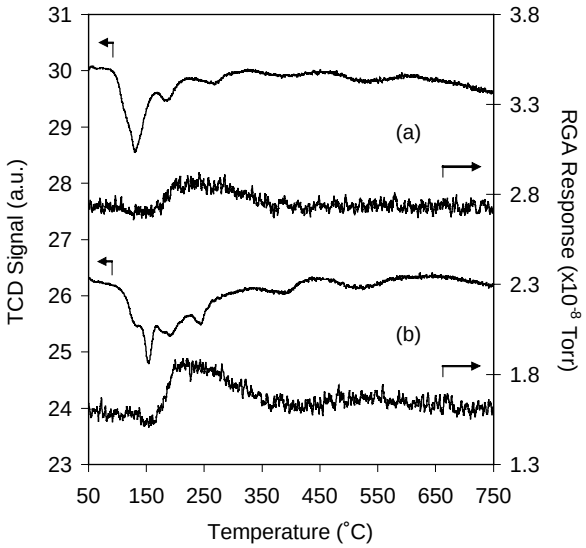

Fig. 3. TCD signal and RGA response (m/z = 18) of (a) $Ce_{0.8}Zr_{0.2}O_2$/Cu-ZSM-5 and (b) $Ce_{0.8}Sm_{0.2}O_{1.9}$/Cu-ZSM-5 during temperature programmed reduction with H_2 (4%) in Ar.

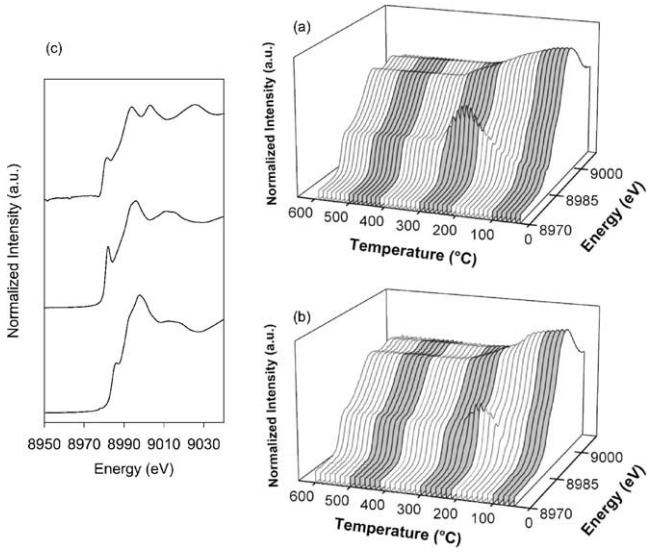

Fig. 4. TPR of (a) Cu-ZSM-5 and (b) CeO_2/Cu-ZSM-5 as detected by the Cu-K edge in XANES. The peak at 8983 eV corresponds to Cu^{1+}. Insert (c) displays the XANES profile from top to bottom of Cu foil, Cu_2O and CuO.

H_2-TPR, is shown in Fig. 4. The different oxidation states of copper have unique features in the XANES region (Fig. 4c) [7]. Cu^{2+} shows a single peak just in the post-edge region with a very weak pre-edge feature at 8785 eV. A strong pre-edge feature dominates the Cu^{1+} XANES spectra at 8983 eV and Cu^0 shows a doublet after the edge and some weak features. Visual inspection of these XANES traces easily shows the transformation of $Cu^{2+} \rightarrow Cu^{1+} \rightarrow Cu^0$ at expected temperatures for Cu-ZSM-5. A comparison between the waterfall plots indicates that, in the case of CeO_2/Cu-ZSM-5, both Cu redox transitions ($Cu^{2+} \rightarrow Cu^{1+} \rightarrow Cu^0$) occur at least at 50 °C lower temperatures.

Similar XANES experiments monitoring the Ce-L_3 edge of CeO_2/H-ZSM-5 and CeO_2/Cu-ZSM-5 are shown in Fig. 5. Ce^{4+} shows a strong doublet in the post-edge region while Ce^{3+} is comprised of only a single peak (Fig. 5c). As with the Cu XANES, the transformation from Ce^{4+} to a mixed oxidation state is apparent for both samples. For the CeO_2/H-ZSM-5 sample, this reduction starts near 400 °C, in agreement with the previous H_2-TPR runs. For the bifunctional sample, the reduction appears to start near 275–300 °C and is completed by 350 °C.

3.4. DRIFTS

3.4.1. CO adsorption

Carbon monoxide is a well-documented probe molecule for Cu-ZSM-5 in infrared spectroscopy. A sharp characteristic band at 2156 cm^{-1} corresponding to the Cu^{1+}(C–O) asymmetric stretching [ν_{as}(CO)] in ZSM-5 is typically used to monitor the state of the active copper site [9]. In this experiments, all ν(CO) bands correspond to the monocarbonyl complex since, at the conditions tested, the dicarbonyl

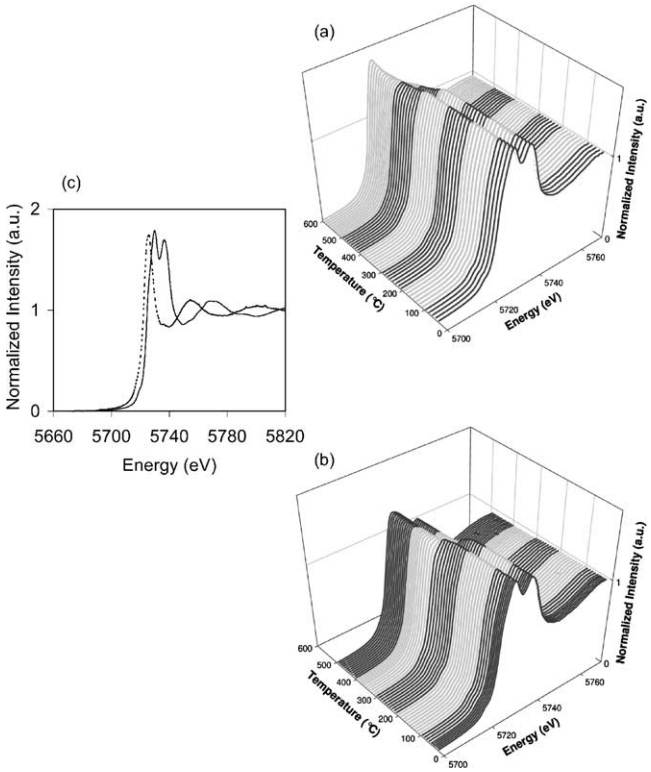

Fig. 5. TPR of (a) CeO_2/H-ZSM-5 and (b) CeO_2/Cu-ZSM-5 as detected by the Ce-L_3 edge in XANES. The insert (c) shows the XANES absorption profile for CeO_2 (solid line) and $Ce(NO_3)_3$ (dotted line).

complex [$Cu^{1+}(CO)_2$]-ZSM-5 is not formed ($Cu^{1+}(C–O)_2$ symmetric stretching $\nu_{sym}(CO) = 2177\,cm^{-1}$). Fig. 6 shows the stability of the Cu^{1+}–CO in Cu-ZSM-5 and CeO_2/Cu-ZSM-5 formed under a constant dry feed of carbon monoxide and oxygen. In general terms, the carbonyl

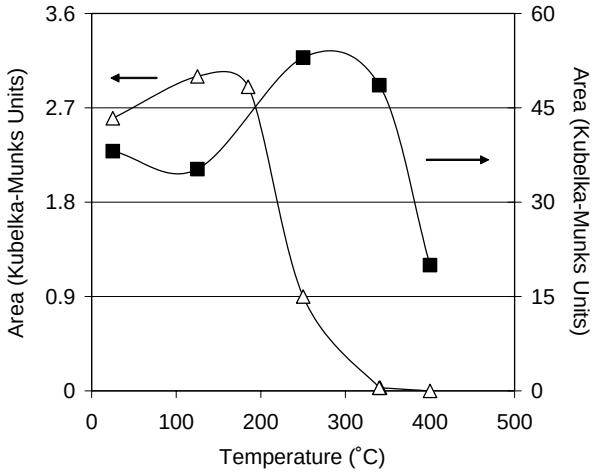

Fig. 6. Relative intensity of the ν(CO) band at 2156 cm^{-1} as a function of temperature for (■) Cu-ZSM-5 and (△) CeO_2/Cu-ZSM-5 as estimated from the area of the peak in Kubelka–Munk units. The lower signal in CeO_2/Cu-ZSM-5 is attributed in part to the lower penetration into the zeolite of the infrared beam due to the ceria coating. Conditions: 1000 ppm CO, 8% O_2, balance N_2, flow 100 sccm.

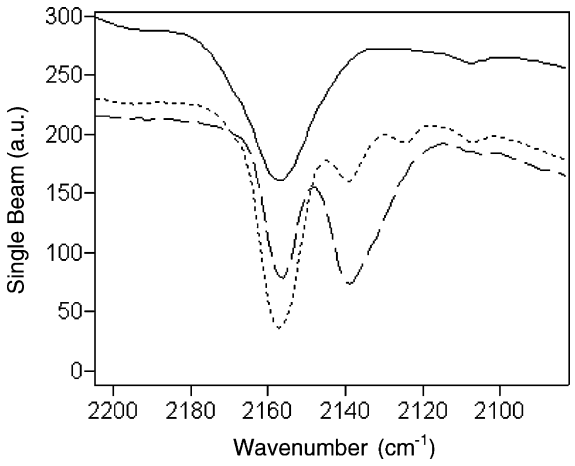

Fig. 7. Typical vibration modes of CO on Cu-ZSM-5 as assigned by Sárkány: $Cu(H_2O)_2(C–O) = 2124\,cm^{-1}$, $Cu(H_2O)(C–O) = 2138\,cm^{-1}$, $Cu(C–O) = 2156\,cm^{-1}$. The small band at $2107\,cm^{-1}$ corresponds to $Cu(^{13}C–O)$. Solid line: catalyst flushed with dry N_2 at 250 °C. Dashed line: flushed with dry N_2 at room temperature. Dotted line: exposed to air at room temperature.

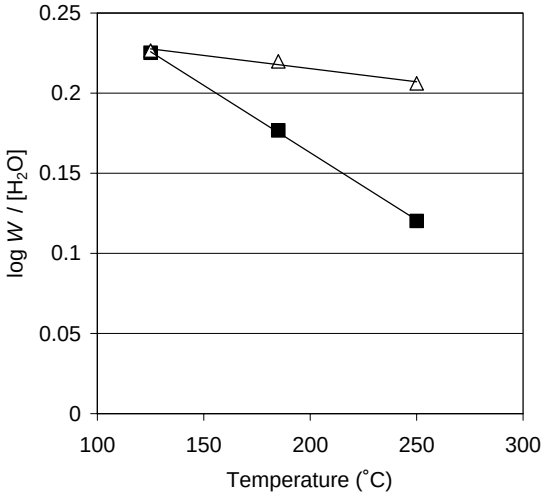

Fig. 8. Variation with temperature of the fraction of hydrated Cu^{1+} per unit of water in the stream in (■) Cu-ZSM-5 and (△) CeO_2-Cu-ZSM-5, as determined by DRIFTS.

formation is favored above 100 °C until the CO is dissociated. It is evident that in the CeO_2-coated catalyst, the copper carbonyl complex is less stable in oxygen than in Cu-ZSM-5. In the absence of oxygen, no decomposition is observed in either catalyst throughout the temperature range studied.

If 6% water is introduced along oxygen and carbon monoxide, the decomposition of the carbonyl complex occurs at lower temperatures, clearly showing a promotion of the carbonyl decomposition by water.

3.4.2. $CO + H_2O$ adsorption

Unlike CO, H_2O produces a broad band in the infrared spectrum that is difficult to quantify in diffuse reflectance IR. However, H_2O co-adsorbed on copper carbonyl in ZSM-5 produces a characteristic red shift of the ν(CO) vibration mode. Fig. 7 shows the typical vibration modes for hydrated carbonyls as assigned by Sárkány [9]. By integrating the area of the Kubelka–Munk (KM) peaks observed during a run involving heating the sample in 1000 ppm of CO and 6–8% H_2O feed, the relative hydration level of the sites can be monitored. Fig. 8 shows the change in hydration as the temperature is increased to 250 °C, where W stands for the % of hydrated Cu^{1+}-carbonyls calculated as follows:

$$W = \frac{\text{KM area of } \nu_{CO} \text{ at } 2138\,cm^{-1}}{\text{KM area of } (\nu_{CO} \text{ at } 2138\,cm^{-1} + \nu_{CO} \text{ at } 2156\,cm^{-1})} \times 100\%$$

and $[H_2O]$ stands for the water composition in the feed. Even though both samples, as expected, lose water as the temperature is increased, the logarithmic plot reveals that more hydrated carbonyls are retained at higher temperatures in the case of the coated CeO_2/Cu-ZSM-5 catalyst.

3.4.3. C_3H_6-SCR

The use of a typical C_3H_6-SCR feed over a catalyst in DRIFTS to monitor in situ the formation of intermediates of the reaction has been demonstrated [10]. In the case of Cu-ZSM-5, a lot of attention in the literature has been directed towards the absorption bands around 2200–2300 cm^{-1} assigned to isocyanate species associated with the support and the Cu sites [11]. When 1000 ppm C_3H_6, 1000 ppm NO and 8% O_2 in nitrogen are fed, both samples, Cu-ZSM-5 and CeO_2/Cu-ZSM-5, display a band at $2255\,cm^{-1}$, in agreement with the literature. However, in the case of the coated catalyst, this band is only observed up to 250 °C. In the native Cu-ZSM-5 that band appears even at 400 °C, which is the maximum temperature the setup used can achieve under the conditions used.

Fig. 9 shows the CO_2 formation on the catalysts at different temperatures, based on the areas of the Kubelka–Munk peaks observed at 2360 and $2330\,cm^{-1}$. The ceria-coated catalyst yields CO_2 as early as 155 °C and its concentration maximizes around 200–250 °C. CO is not observed in the temperature range examined. The native Cu-ZSM-5 does not yield detectable amounts of CO_2 at 250 °C or below and produces significant amounts of CO at 400 °C. These results indicate that the ceria-coated material activates the hydrocarbon at lower temperatures and oxidizes it more efficiently.

3.5. TGA and TPD

The weight loss of the catalysts in a N_2 flow as a function of temperature is presented in Fig. 10a. Temperature programmed desorption (TPD) of water by the catalysts in He is also shown in Fig. 10b. The first plot indicates a higher absorption of water by the coated catalyst while the second

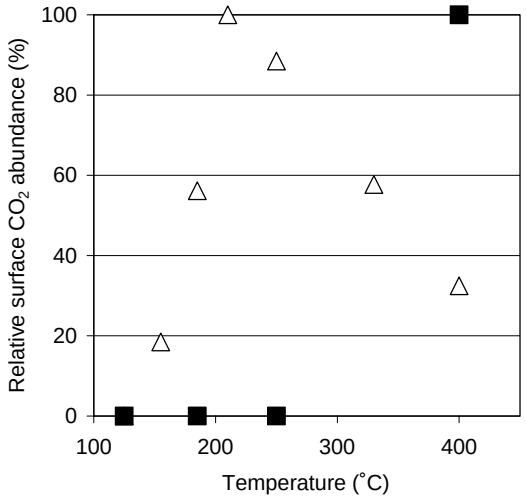

Fig. 9. Observed surface CO_2 during C_3H_6-SCR as detected in situ with DRIFTS: (■) Cu-ZSM-5, (△) CeO_2-Cu-ZSM-5. CO is also observed at 400 °C in Cu-ZSM-5. No significant amounts of CO are detected in CeO_2/Cu-ZSM-5 in the temperature range examined.

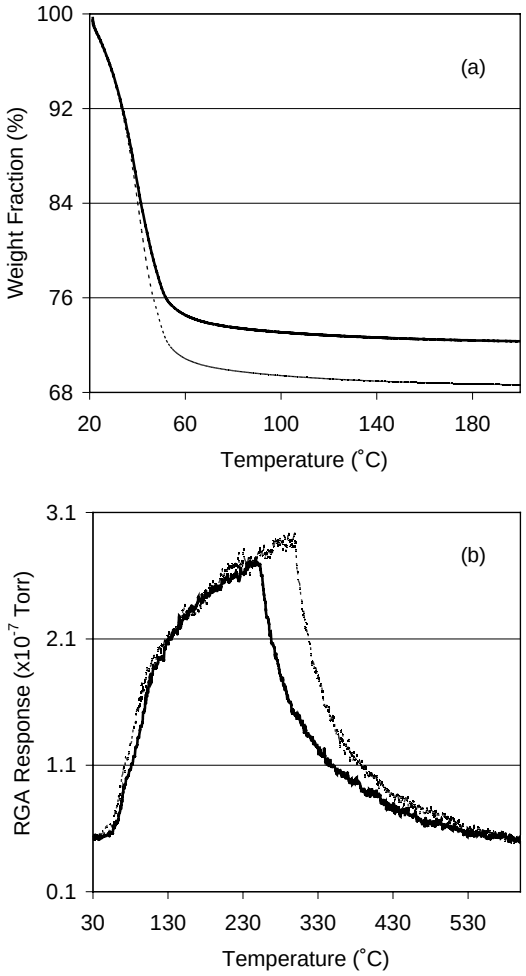

Fig. 10. (a) Weight loss of the catalysts exposed to a water-saturated controlled environment as determined by TGA. (b) Water desorption of the catalysts as a function of temperature as determined by RGA ($m/z = 18$) during TPD in He. Solid dark line: Cu-ZSM-5, dashed light line: CeO_2/Cu-ZSM-5.

plot indicates a longer retention of water molecules by this catalyst as the temperature is ramped up.

4. Discussion

In general, the catalysts prepared follow the trends normally observed for HC-SCR catalysts: The hydrocarbon is activated first. NO conversion begins at higher temperatures. As the temperature is increased further, the NO and hydrocarbon conversions increase. This trend continues until nearly 100% hydrocarbon conversion is reached. From that point on the NO conversion typically drops and the selectivity towards NO_2 increases. This behavior can be generally explained following a simplistic model in which the hydrocarbon is activated by O_2 and NO is oxidized to NO_2. NO_2 can, in turn, react with a surface-activated hydrocarbon species to produce N_2, CO_2 and H_2O [12]. As the temperature increases, the total oxidation of the hydrocarbon by O_2 becomes more favorable and some unreacted NO_2 starts to evolve pass the catalyst. In addition, the NO oxidation reaction is exothermic and decreases with temperature as mandated by thermodynamics. A plateau is reached above 500 °C where the activity is due mainly to the direct but less favorable reaction between NO and the activated hydrocarbon.

The CeO_2/Cu-ZSM-5 catalyst displays most of this behavior at lower temperatures than plain Cu-ZSM-5. Ceria is known for promoting oxidation reactions. The lower temperature effect in the bifunctional catalyst could arise from ceria being able to reduce the temperature at which NO_2 is formed and match it to the temperature at which propylene is activated. This effect maximizes the total NO conversion window between the hydrocarbon activation and the NO_2 thermal decomposition (Fig. 1b). In the high temperature end of the window the selectivity towards NO_2 is higher relative to Cu-ZSM-5 since ceria also promotes the competing reaction of the hydrocarbon with oxygen at lower temperatures. However, as reported earlier, a simple mixture of ceria and Cu-ZSM-5 shows only limited temperature benefits compared to the coated CeO_2/Cu-ZSM-5 [6]. In addition, the effect of ceria on those two reactions alone does not explain the improvement in activity when water is added to the system.

4.1. Interaction of Ce and Cu

Results obtained by TPR and XAS definitely show an interaction between copper and cerium atoms. H_2-TPR experiments reveal a new hydrogen absorption event at low temperatures (150 °C) not displayed by the individual phases of the catalyst or by CeO_2/H-ZSM-5. This low temperature peak resembles those observed in the H_2-TPR of doped ceria [13]. In particular, doping of ceria with CuO has been found to increase the reducibility of ceria significantly [14]. It is conceivable that copper present at the zeolite–oxide in-

terface may act as dopant of the ceria crystals. Although no evidence of such a mixed oxide phase is found on the XRD traces of the bifunctional catalysts [6], its presence cannot be eliminated. A Cu-doped ceria phase would be difficult to observe by XRD in the heavily ceria-coated catalyst given the similarity between its lattice structure and that of plain ceria. In addition, the expected short-range order of the modified lattice would make the doped phase even harder to detect by this technique. Other groups have shown that, below 5 at.% Cu, the diffraction patterns of the Cu-doped CeO_2 and pure CeO_2 are almost identical [14,15]. On the other hand, in situ XANES analysis allows the direct observation of the state of both metals during a similar temperature programmed reduction with H_2. The results shown in Figs. 4 and 5 confirm the proposed Ce–Cu interaction. Not only is the cerium reducibility drastically affected when in contact with Cu-ZSM-5 (partial reduction of ceria occurs at 100–125 °C lower temperature than in CeO_2/H-ZSM-5) but also the copper redox transitions take place at lower temperatures in the bifunctional catalyst relative to Cu-ZSM-5. The fact that, in the case of cerium, only a partial reduction is observed is in agreement with a model of two different types of cerium atoms: those on the interface actually interacting with the zeolite and those on the external ceria crystals of the coating. Thus, the reducibility of a significant fraction of both metals (Cu and Ce) appeared to have been modified during the coating procedure. It is unclear if the higher reducibility of Cu comes from the same Ce–Cu interaction that lowers the redox potential of Ce. Still, the ability to be reduced at lower temperatures is a relevant catalyst benefit since the oxidative activation of NO and the hydrocarbon can take place at lower temperatures and thus shift the overall HC-SCR activity.

In solid oxide fuel cells, doping ceria with samarium or zirconium increases the oxygen ion conductivity of ceria [16]. However, while zirconium increases the reducibility of ceria, samarium decreases it [16,17]. Hence, the use of doped ceria as coating material in the bifunctional catalysts could affect the NO and/or propylene activation temperature and, in consequence, the temperature of maximum SCR activity. Surprisingly, the test performed show that doping ceria with samarium or zirconium does not affect the activity window of the coated catalysts significantly (Fig. 11), despite adding low temperature features to the H_2-TPR shown in Fig. 3. In addition, in situ XANES-TPR monitoring the Cu-K edge of CeO_2/Cu-ZSM-5 and $Ce_{0.8}Sm_{0.2}O_{1.9}$/Cu-ZSM-5 (not shown) displays no significant difference in copper reducibility between the two samples. This is consistent with a model where discrete Cu–Ce atomic interactions are responsible for the lower temperature catalyst activity rather than the bulk of the ceria crystals. These results also imply that the quality of the ceria, typically contaminated with other rare-earth metals, is not crucial in the preparation of these materials.

DRIFTS provides a good marker for the presence of Cu^{1+} carbonyl complex since no carbonyl of Cu^{2+} can be formed

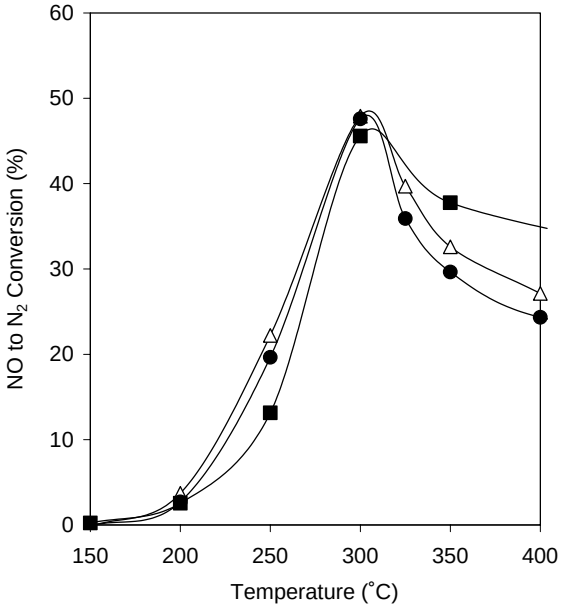

Fig. 11. Effect of doping ceria on NO to N_2 conversions: (△) CeO_2 (12%)/Cu-ZSM-5, (●) $Ce_{0.8}Zr_{0.2}O_2$ (15%)/Cu-ZSM-5 and (■) $Ce_{0.8}Sm_{0.2}O_{1.9}$ (10%)/Cu-ZSM-5. Conditions: 1000 ppm NO, 1000 ppm C_3H_6, 2% O_2, balance He at GHSV = 40,000 h^{-1} (based on mass of catalyst). Notice the higher temperature of activity due to the lower ceria content in all samples.

at the applied conditions [18]. In general, the thermal decomposition of the carbonyl complex displayed in Fig. 6 could occur via two mechanisms: the oxidation of CO into CO_2 and/or the oxidation of Cu^{1+} to Cu^{2+}. In the case of Cu-ZSM-5, no CO_2 band is observed in DRIFTS up to the temperature where the carbonyl is fully decomposed. The stability in 8% O_2 as a function of temperature of pre-formed copper carbonyl in Cu-ZSM-5, in the absence of a CO feed, is shown in Fig. 12. Also shown in the same figure is the transition of Cu^{1+} to Cu^{2+}, as determined by factor analysis of the XANES spectra collected during O_2-TPO of Cu-ZSM-5. The close match between the two profiles suggests that in the case of Cu-ZSM-5, the decomposition of the carbonyl is due mostly to the oxidation of Cu^{1+}.

The results of Fig. 6 indicate that the copper carbonyl complex loses thermal stability with the addition of the ceria coating. While factor analysis of the XANES spectra collected during O_2-TPO of CeO_2/Cu-ZSM-5 (not shown) indicates that the oxidation temperature of Cu^{1+} is lower with the addition of ceria, the profile does not match the thermal stability of the carbonyl in this sample. The carbonyl decomposes at lower temperatures than expected. At the same time, DRIFTS reveals the formation of CO_2 on CeO_2/Cu-ZSM-5 as low as 185 °C during the carbonyl decomposition through the appearance of a weak absorption band at 2360 cm^{-1}. Hence, in the case of the ceria-coated sample, the decomposition of the Cu–CO complex is due to the oxidation of both, Cu^{1+} and CO. This is in agreement with the results obtained during the in situ DRIFTS analysis under C_3H_6-SCR conditions, which indicate that the CeO_2-coated system

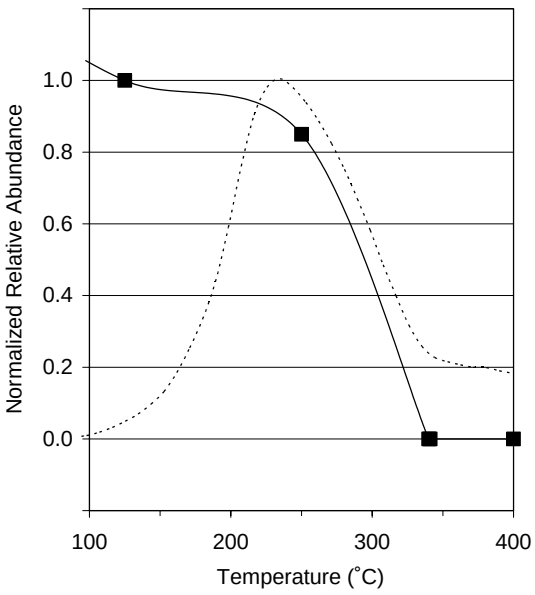

Fig. 12. Comparison between the relative abundance as a function of temperature of Cu^{1+}–CO under 8% O_2 (as determined by DRIFTS) (■) and Cu^{1+} (as determined by factor analysis of XANES spectra) during O_2-TPO (dotted line). DRIFTS values below 100 °C are affected by water co-adsorption and are not considered in the plot.

efficiently combusts propylene at temperatures lower than 200 °C (Fig. 9). The fact that CeO_2/Cu-ZSM-5, unlike the native Cu-ZSM-5, does not produce detectable amounts of by-products such as CO and N_2O during C_3H_6-SCR conditions is also explained by the results of the latter experiment.

4.2. Water effect

Water has been reported to lower the temperature of maximum activity of highly exchanged Cu-ZSM-5 [19]. Both Cu-ZSM-5 and CeO_2/Cu-ZSM-5 display a 50 °C temperature drop in the activity maximum in the presence of water [6]. When copper carbonyl is formed in either sample, CO can slowly be displaced by water over time. However, if CO is continuously fed in the wet stream, equilibrium is reached and the carbonyl remains stable at temperatures higher than 250 °C even in the case of CeO_2/Cu-ZSM-5. When oxygen is introduced, the copper carbonyl decomposes quickly above 185 °C in the case of the ceria-coated catalyst while the carbonyl formed on plain Cu-ZSM-5 shows little change. Fig. 13 shows the CO and CO_2 stretching bands observed on CeO_2/Cu-ZSM-5 in the presence of CO and oxygen with and without water. It is clear that the decomposition of the carbonyl is promoted by water. Interestingly, less CO_2 is observed when water is added. This suggests that water mainly promotes the oxidation of Cu^{1+} rather than the oxidation of CO. At the conditions studied, this effect is not observed in the Cu-ZSM-5 sample since at the temperatures where water can still be seen adsorbed on the catalyst (<250 °C), the carbonyl formed in Cu-ZSM-5 is still stable (Fig. 6). The promotional effect of water over the oxidation of copper can enhance the deNO_x activity of the catalyst at lower temperatures by assisting the regeneration of the active sites for the NO to NO_2 reaction step.

Unlike Cu-ZSM-5, CeO_2/Cu-ZSM-5 displays higher NO_x to N_2 conversion in the presence of water than under dry conditions. The results displayed in Fig. 8 indicate that a larger fraction of water molecules remain in the copper active sites of the ceria-coated catalyst at temperatures where the catalyst is active for NO reduction. The higher temperature desorption profile of water under a He flow displayed by the bulk of the coated sample in Fig. 10b during TPD is in agreement with the results obtained for the active sites by DRIFTS. In addition, the higher affinity of the bifunctional CeO_2/Cu-ZSM-5 catalyst towards water is confirmed by the TGA results in Fig. 10a, which shows that the coated sample absorbs larger amounts of water than Cu-ZSM-5 under comparable conditions. Hence, it is proposed that the activity promotion effect by water is greatly enhanced in the coated CeO_2/Cu-ZSM-5 since this system, in contrast with

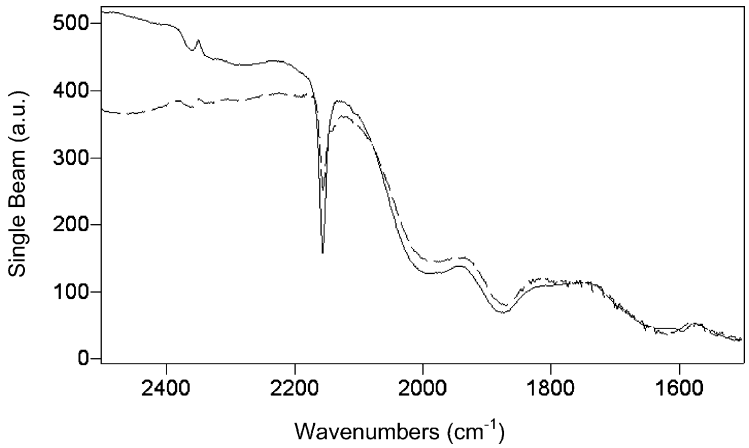

Fig. 13. Effect of water in the presence of oxygen on the stability of the Cu^{1+}–CO complex on CeO_2/Cu-ZSM-5. The sharp peak at 2156 cm^{-1} corresponds to the CO stretching vibration in the complex. The weak peak at 2360 cm^{-1} corresponds to CO_2. Solid line: dry run. Dashed line: 6% water introduced. Conditions: 1000 ppm CO, 8% O_2, N_2 balance, flow = 100 sccm, temperature 185 °C. The same water effect is not observed in the absence of oxygen.

others, performs at a low temperature range where water molecules can still co-exist on the active sites.

The CeO_2/Cu-ZSM-5 catalyst also shows higher stability towards hydrothermal decomposition relative to the native Cu-ZSM-5 [6]. This is not surprising since the addition of cerium or lanthanum ions to Cu-ZSM-5 has already been shown to create stability towards steam induced degradation of zeolitic systems [20]. In the particular case of cerium, when this ion is exchanged in the zeolite prior to copper, no stabilization is observed [20]. However, when the order of metal exchange is reversed, the catalyst retains some deNO_x activity even after extreme steaming conditions (20% water content in the feed at 600 °C) [21]. While in the first procedure cerium is believed to remain inside the zeolite pores as Ce^{3+} or small oxide particles, in the second procedure the authors have reported that a fraction of the added cerium atoms may be found as ceria (CeO_2) on the outer surface. In the case of the coated CeO_2/Cu-ZSM-5, the improvement in water stability must be due to the presence of the ceria strictly on the external surface of the zeolite since no significant amount of cerium ions are expected to dissolve and penetrate the pores. DRIFTS results in Fig. 8 show that as the temperature is increased, less water is retained by the active sites. At 600 °C the hydrophilicity of ceria relative to the zeolite shown by TGA may attract the water molecules and limit the rate at which water enters the zeolite, and that way, limit the damage to the zeolite structure.

5. Conclusions

The technique of coating the zeolite samples with nano-sized oxides provides additional benefits relative to other combination techniques reported in the literature including co-exchange and physical mixtures of the components. In general the addition of cerium to Cu-ZSM-5 and other zeolites can activate NO and propylene at lower temperatures. The notably larger drop in the temperature for maximum activity displayed by the coated CeO_2/Cu-ZSM-5 relative to other Ce-zeolite systems is explained by the higher reducibility of both Cu and Ce. The effect on cerium is proposed to be due to the chemical interaction (as opposed to physical) of copper atoms with ceria nanoparticles. The copper atoms in the oxide–zeolite interface are affected by both environments, giving the surface active sites of the zeolite unique properties. The full surface coverage offered by the ceria layer maximizes this dual environment interaction and hence, the low temperature oxidation of NO to NO_2.

The addition of water also promotes the reaction at lower temperatures, probably by assisting the regenerative oxidation of Cu^{1+}. Since the ceria layer in the coated CeO_2/Cu-ZSM-5 catalyst retains water at the interface during reaction conditions, the low temperature conversion is enhanced even further. Cu-ZSM-5 is unable to reproduce this water enhancement effect since the reduction of NO_x occurs at temperatures at which water is poorly adsorbed by the unmodified catalyst. The affinity of the ceria coating towards water protects the internal zeolite in CeO_2/Cu-ZSM-5 against hydrothermal degradation by restricting the diffusion of water molecules into the zeolite pores.

Acknowledgements

This work was performed under the auspices of the Argonne National Laboratory “Laboratory Director’s Research and Development” program under contract number W-31-109-ENG-38. Additional funding support was provided by the BP Corporation. Work performed at MR-CAT was supported, in part, by funding from the Department of Energy under grant number DEFG0200ER45811.

References

[1] M. Guyon, V. LeChanu, P. Gilot, H. Kessler, G. Prado, Appl. Catal. B: Environ. 8 (1996) 183.
[2] R. Burch, T.C. Watling, Appl. Catal. B: Environ. 11 (1997) 207.
[3] Y.P. Zhang, M. Flytzani-Stephanopoulos, in: J.N. Armor (Ed.), Environmental Catalysis, American Chemical Society, Washington, DC, 1994, p. 7.
[4] Z.J. Li, M. Flytzani-Stephanopoulos, Appl. Catal. A: General 165 (1997) 15.
[5] H. Berndt, F.W. Schutze, M. Richter, T. Sowade, W. Grunert, Appl. Catal. B: Environ. 40 (2003) 51.
[6] M.K. Neylon, M.J. Castagnola, N.B. Castagnola, C.L. Marshall, Catal. Today 96 (2004) 53.
[7] M.K. Neylon, C.L. Marshall, A.J. Kropf, J. Am. Chem. Soc. 124 (2002) 5457.
[8] E.R. Malinowski, Factor Analysis in Chemistry, Wiley, New York, 1991.
[9] J. Sárkány, Appl. Catal. A: General 229 (2002) 291–312.
[10] I.C. Hwang, D.H. Kim, S.I. Woo, Catal. Lett. 42 (1996) 177.
[11] F. Solymosi, T. Bansagi, J. Catal. 156 (1995) 75.
[12] M. Guyon, B.R. Stanmore, P. Gilot, Chem. Comm. (1996) 1227.
[13] Q. Fu, S. Kudriavtseva, H. Saltsburg, M. Flytzani-Stephanopoulos, Chem. Eng. J. 93 (2003) 41.
[14] M.F. Luo, Y.J. Zhong, X.X. Yuan, X.M. Zheng, Appl. Catal. A: General 162 (1997) 121.
[15] P. Bera, K.R. Priolkar, P.R. Sarode, M.S. Hegde, S. Emura, R. Kumashiro, N.P. Lalla, Chem. Mater. 14 (2002) 3591.
[16] H. Yahiro, Y. Eguchi, K. Eguchi, H. Arai, J. Appl. Electrochem. 18 (1988) 527.
[17] S. Zhao, R.J. Gorte, Appl. Catal. A: General 248 (2003) 9.
[18] K. Hadjiivanov, H. Knozinger, J. Catal. 191 (2000) 480.
[19] C. TorreAbreu, M.F. Ribeiro, C. Henriques, F.R. Ribeiro, G. Delahay, Catal. Lett. 43 (1997) 31.
[20] P. Budi, E. CurryHyde, R.F. Howe, Catal. Lett. 41 (1996) 47.
[21] Y.P. Zhang, M. Flytzani-Stephanopoulos, J. Catal. 164 (1996) 131.